SAE TECHNICAL PAPER SERIES

2002-01-3337

An Experimentally Validated Physical Model of a High-Performance Mono-Tube Damper

Michael S. Talbott
Honda R&D Americas, Inc.

John Starkey
Purdue University

Reprinted From: Proceedings of the 2002 SAE Motorsports Engineering Conference and Exhibition (P-382)

Motorsports Engineering Conference & Exhibition
Indianapolis, Indiana
December 2-5, 2002

400 Commonwealth Drive, Warrendale, PA 15096-0001 U.S.A. Tel: (724) 776-4841 Fax: (724) 776-5760 Web: www.sae.org

ISSN 0148-7191

Printed in USA

2002-01-3337

An Experimentally Validated Physical Model of a High-Performance Mono-Tube Damper

Michael S. Talbott
Honda R&D Americas, Inc.

John Starkey
Purdue University

ABSTRACT

A mathematical model of a gas-charged mono-tube racing damper is presented. The model includes bleed orifice, piston leakage, and shim stack flows. It also includes models of the floating piston and the stiffness characteristics of the shim stacks. The model is validated with experimental tests on an Ohlins WCJ 22/6 damper and shown to be accurate. The model is exercised to show the effects of tuning on damper performance. The important results of the exercise are 1) the pressure variation on the compression side of the piston is insignificant relative to that on the rebound side because of the gas charge, 2) valve shim stiffness can be successfully modeled using stacked thin circular plates, 3) bleed orifice settings dominate the low speed regime, and 4) shim stack stiffness dominates the high speed regime.

INTRODUCTION

The ability to tune a damper quickly without testing is of great interest in motorsports. Damper engineers often try several combinations of valve shims, piston orifices, and bleed orifices before finding the right combination for a particular setup on the car. The nature of the dampers used in motorsports also lends to a study of their physics. Whereas a production automobile damper's performance characteristics are fixed by its construction, a motorsports damper is highly tunable through external adjustments and by varying internal components. This feature makes motorsport dampers well suited to a study of their physics.

A great deal of work has been done in developing empirical models (Duym, et. al., 1997, Reybrouck, 1994), each of which is valid for one configuration of a particular damper. However, little has been done to produce an analytical model that contains those parameters used by engineers to tune a suspension damper to a particular vehicle or road condition.

The goal of this paper is to develop an accurate damper model based on the physics involved within the damper. In order to accomplish this, the first step is to understand the physics that govern damper behavior. With a preliminary understanding of the physics, it is then possible to identify those parameters that have the greatest influence on damper performance, which leads to a model focusing on those parameters. Once the model is then correlated to experimental data, the model can be exercised to gain even greater understanding of the relationship between damper design parameters and damper performance.

BACKGROUND

For this study the focus will be on hydraulic, single tube, telescopic dampers, specifically a NASCAR type damper. Figure 1 depicts a typical, NASCAR, single tube damper. The mono-tube damper is the preferred construction in racing applications.

The damper consists of several main parts. The tube of the damper houses all of the internal components. Once assembled, the tube is divided into three chambers: gas, rebound, and compression. The gas chamber is at the top of the tube; it is separated from the compression chamber by a floating piston. This piston separates the gas in the gas chamber, typically nitrogen, from the oil in the compression chamber. The compression chamber sits between the floating piston of the gas chamber and the piston. The rebound chamber is opposite the compression chamber on the other side of the piston and at the bottom end of the tube. Both the compression chamber and rebound chamber are completely filled with high-quality mineral or synthetic oil. The piston of the damper is connected to the rod that goes through the rebound chamber and out the bottom of the tube. The rod passes through a special seal designed to keep the oil in, dirt out and to minimize friction between the rod and seal. The damper is attached to the vehicle through two eyelets.

The damper operates in two modes, compression (positive velocity) and rebound (negative velocity). During the compression stroke the rod is pushed into the tube and fluid flows through the piston from the compression chamber to the rebound chamber. The rebound stroke is the reverse process in which the rod is drawn out of the tube and fluid flows from the rebound chamber to the compression chamber.

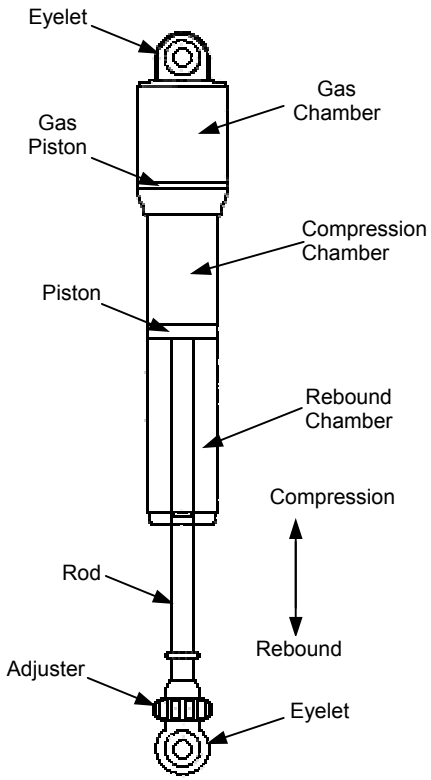

Figure 1: Major Components of a NASCAR Mono-Tube Damper.

The main mechanism for providing damping is by shearing the hydraulic fluid as it flows through restrictions. This dissipates energy by generating heat in the fluid that is then dissipated to the shock tube and then to the atmosphere. The other mechanism for damping is friction between the various moving parts of the damper. A great deal of design effort goes into trying to keep the friction as low as possible because it is a force component that is relatively independent of velocity.

Since the primary damping mechanism is directly proportional to the flow restrictions, it is clear that these restrictions are very important in damper performance. Total fluid flow is split among three possible paths. The first is through the bleed orifice located in the end of the rod (See label 3 in Figures 2 and 3). Fluid can flow through this orifice at all piston speeds from the compression to rebound chamber and vice versa. The bleed orifice dominates the low speed characteristics of the damper. The area of the orifice can be adjusted by screwing a needle valve in and out.

The second flow passage is through the rebound or compression valves on the piston. Label (1) in Figure 2 and label (2) in Figure 3 depict fluid flow through the rebound valve and compression valve respectively. These valves are essentially check valves that allow flow in only one direction. Each valve consists of an orifice in the piston and a shim stack. The shim stack is a series of thin circular steel discs stacked according to diameter. Figure 2 shows the rebound shim stack and rebound piston orifice. The combination of the piston orifice and the annular flow path created by deflecting the shim stack puts two flow resistances in series. The damper is usually designed so that the annular flow area around the valve stacks, and not the piston orifices, dominate the flow resistance. However, at very high piston velocities the piston orifices can dominate the flow resistance, and are thus an important damper design characteristic.

The shim stack is effectively a spring-loaded plate that blocks the piston orifice unless a pressure differential exists. The stacks are typically preloaded by dishing the piston slightly. This preload prevents the stack from opening until the pressure differential reaches a desired level. To correctly calculate the flow through the valve, it is necessary to know the deflection of the shim stack for a given pressure differential. Modeling of the shim stack is not a trivial problem and is an important contribution of this paper.

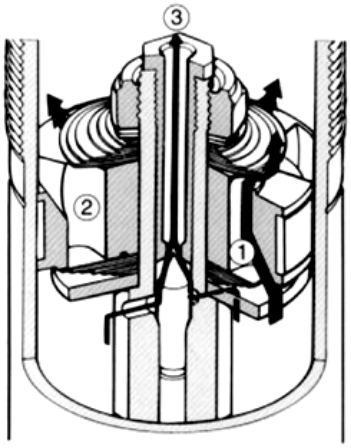

Figure 2: Cutaway Showing Flow Paths Through the Rebound Piston Orifice and Shim Stack (1) and Through the Bleed Orifice (3), During the Rebound Stroke.

The compression valve is located on the rebound side of the piston. It is conceptually the same as the rebound valve, but the piston orifice diameter and the shim stack configuration can be different from the rebound valve. Figure 3, shows the flow paths during the compression stroke.

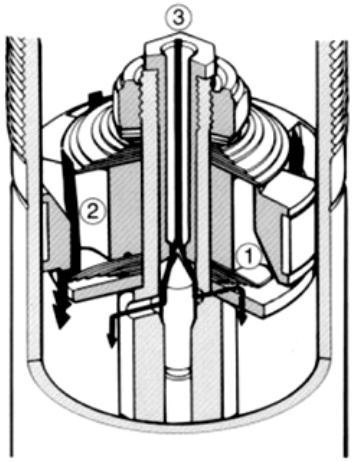

Figure 3: Cutaway Showing Flow Paths Through the Compression Piston Orifice and Shim Stack (2) and Through the Bleed Orifice (3), During the Compression Stroke.

The final flow path is leakage between the piston ring and tube wall. While this is undesirable, it is very difficult to prevent altogether. The effect of leakage on damper performance is minimal unless the leakage becomes significant relative to the other flow paths, at which time the piston-sealing ring should be replaced. However, this flow path is included in the mathematical model presented here.

A floating piston separates the compression chamber from the gas chamber. The gas chamber contains pressurized gas, usually air or nitrogen. Dried nitrogen is preferred because it is more stable with temperature changes due to the lack of water vapor.

This pressurized gas chamber keeps the oil in the damper pressurized to prevent cavitation. As will be shown in this paper, the pressure in the compression chamber is dictated by the pressure in the gas chamber. Therefore, to generate a pressure drop across the piston requires the rebound chamber pressure to fluctuate significantly both above and below the gas charge pressure. When the gas pressure is too low, the rebound chamber pressure can drop below the vapor pressure of the oil, leading to cavitation. Cavitation significantly alters the damper performance and can lead to premature component failure.

The gas chamber also accounts for the volume of the rod entering and exiting the tube during piston motion. As the rod enters the tube during compression, the gas will compress and the floating piston will move up to decrease the gas volume by the amount of piston rod volume that has entered the damper body. When the rod is drawn out of the tube, the gas expands and the floating piston moves down.

The pressure in the gas chamber also gives the damper a small gas spring effect. A force equal to the gas pressure times the rod area will always be exerted on the rod. As the rod is inserted further into the tube, the gas pressure increases and therefore, the gas force increases on the rod. The result is a gas spring effect, independent of velocity.

Creating a physics-based model to predict damper performance is difficult. There are numerous dependent factors that affect damper performance including oil viscosity, temperature, bleed and piston orifices, piston valving, and gas pressure. The resulting relationships between those factors are highly non-linear and dependent upon damper velocity, displacement, acceleration, and frequency. Finally, the shape of the flow paths is complicated, making flow modeling difficult. These issues will be discussed in the mathematical model development that follows.

MATHEMATICAL MODEL

Figure 4 shows the essential physical elements needed for a mathematical model of a damper. Without loss of generality, only the compression stroke is illustrated. The compression valve is open allowing flow through the piston. The bleed orifice is also flowing and there is a small amount of leakage past the piston and cylinder wall. The gas piston movement (z) is proportional to the amount of rod insertion (x). The rebound stroke is the reverse of this, with the rebound valve on the compression side of the piston being open and the compression valve closed. Throughout the following model development the damper is in compression unless otherwise noted.

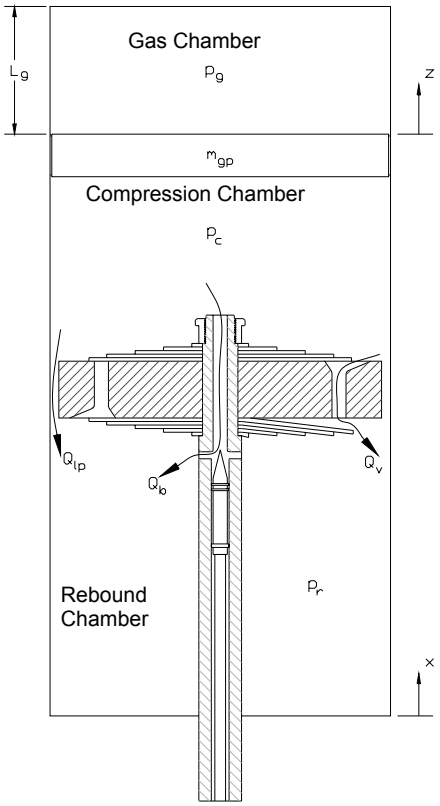

Figure 4: Compression Stroke Diagram Showing the Three Flow Paths (Q_{lp}, Q_b, and Q_v), Pressure Chambers, and the Sign Convention for Piston and Gas Piston Displacements.

To determine the force the damper produces for a given speed, a free-body diagram is constructed for the piston and rod assembly, Figure 5. This is the basis for the mathematical model of the damper. The forces acting on the rod-piston assembly during a cycle are: 1) the pressure force differential across the piston p_rA_r-p_cA_c, and 2) friction F_f between the piston ring and tube and between the rod and the seal. Summing forces on the piston gives:

$$F + p_r A_r - p_c A_c - F_f = m_p \ddot{x} \qquad (1)$$

This equation will be used to solve for the damper force, F, as a function of damper motion (position, velocity, and acceleration). Models must now be derived for each mechanism within the damper affecting the pressures in the rebound and compression chambers, as well as the friction force. It has been shown in previous work that the pressures depend on numerous parameters and inputs including the damper stroke, velocity, and acceleration. To predict the pressures, flow resistance models must be created.

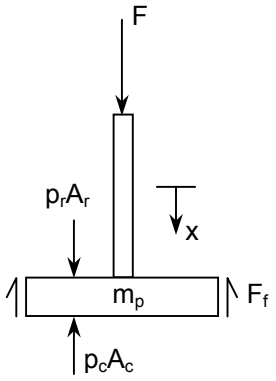

Figure 5: Free-Body Diagram of Piston-rod Assembly.

FLOW SUMMATION

The pressure differential that is generated when the piston is moved depends on restrictions to flow between the rebound and compression chambers. As was discussed in the background section, there are three possible flow paths between the chambers: 1) flow through the bleed orifice, 2) flow through the compression or rebound valve, and 3) leakage between the piston ring and tube. Conservation of mass requires that the fluid that leaves the compression chamber must enter the rebound chamber and vice versa. If it is assumed that the damper oil is incompressible and therefore has a constant density, then a volumetric summation can be used. This concept is illustrated in Figure 6, which depicts the compression stroke.

The total flow rate is made up of three individual flows: flow through the bleed orifice (Q_b), flow through the compression or rebound valve (Q_v), and leakage between the piston ring and tube (Q_{lp}):

$$Q = Q_v + Q_b + Q_{lp} \qquad (2)$$

During compression the gas piston moves right (Figure 6) because $A_c\dot{x} > A_r\dot{x}$. Flow Q' across the fixed boundary B-B is $(A_c - A_r)\dot{x}$. On rebound the gas piston moves left and Q' flows left across B-B, still $Q' = (A_c - A_r)\dot{x}$. This means the area of the rod is accounted for by the gas chamber. Therefore the total flow rate is the piston area, A_r, on the rod side times its velocity:

$$Q = A_r\dot{x} \qquad (3)$$

The individual flow rates must now be calculated, which is the focus of the next section.

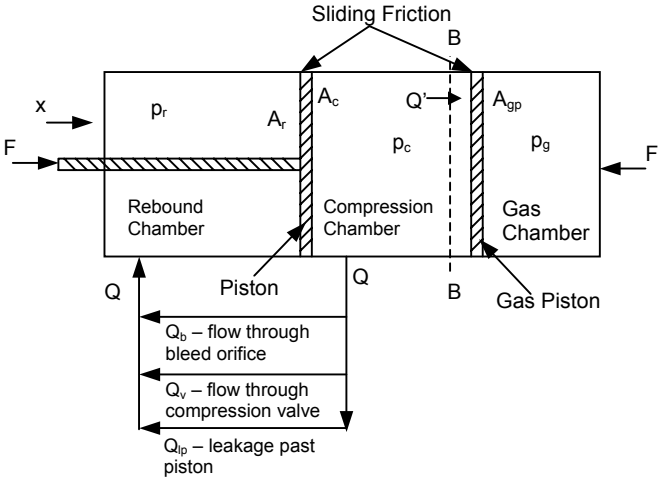

Figure 6: Compression Flow Diagram.

CONSTANT AREA PASSAGE FLOW MODEL

Lang showed that Bernoulli's equation could be used to model the unsteady flow through constant area passages in a damper (Lang, 1977). However, he did make a modification necessary to apply Bernoulli's equation to an unsteady flow. Rather than using a steady-state discharge coefficient, C_d, he defined a dynamic discharge coefficient, C_D, which is a function of the acceleration number, Reynolds number, Cauchy number, and the thickness to length ratio (Lang, 1977):

$$C_D = \phi\left\{\frac{al}{v^2}, \frac{\mu}{\rho v l}, \beta v^2 \rho, \frac{s}{l}\right\} \tag{4}$$

From this, the unsteady flow through a constant area passage is given by:

$$Q = C_D A \sqrt{\frac{2\Delta p}{\rho}} \tag{5}$$

This flow model will be used for flow through the valves and flow through the bleed orifice.

VALVE MODEL

Figure 7 shows a simple model of the valve during the compression stroke. Flow through the valve, Q_v, is associated with the pressure drop between pressures p_c and p_r. However, at least three pressures are needed to describe the flow system because there are two flow resistances in series. The first flow resistance is the piston orifice with area A_o. The pressure drop across the orifice is $p_c - p_v$. The pressure drop across the valve is $p_v - p_r$. The pressure acts on the area of the valve, which generates a force deflecting the shim stack represented by the stiffness k. The flow area of the valve is the circumference of the annular area πD_v times the deflection y of the shim stack, where the diameter of the valve is the diameter of the largest shim in the stack:

$$A_{v,flow} = \frac{1}{2}\pi D_v y \tag{6}$$

Since the piston has three orifices for compression and three for rebound, it is assumed that flow area is one half the total annular area. For compression the pressure differential across the valve is

$$\Delta p_{valve} = p_v - p_r \tag{7}$$

Substituting equations (6) and (7) into (5) yields the final equation for flow through the valving:

$$Q_v = \frac{1}{2}\pi D_v y C_D \sqrt{\frac{2\Delta p_{valve}}{\rho}} \tag{8}$$

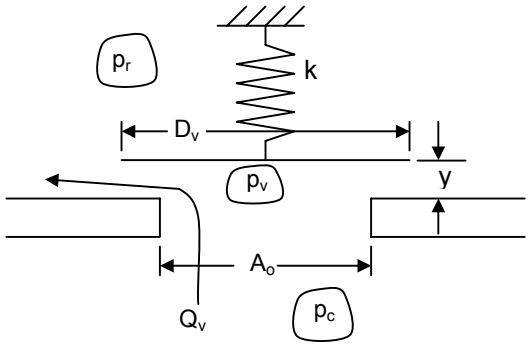

Figure 7: Simple Valve Model (Compression Stroke).

To determine the deflection of the valve, y, it is necessary to know the forces on the valve. Figure 7 depicts the assumed pressure regimes for the valve flow restriction. From this, a free-body diagram can be constructed for the shim stack, Figure 8.

There are four forces acting on the shim stack: the pressure differential times the valve area, $\Delta p_{valve} A_v$; the preload on the shim stack, F_{sp}; the stiffness of the shim stack times the deflection, ky; and a force due to the momentum change of the fluid, F_m. The mass of the valve is neglected.

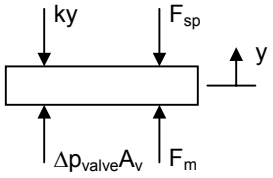

Figure 8: Free-Body Diagram of Valve.

Details about the pressure distribution on the shim stack and how its stiffness is derived are explained later. The preload deflects the shim stack even though the valve is closed. The momentum force results from changing the direction of fluid flow (See Figures 4 and 7). Summing forces on the valve gives:

$$ky = \Delta p_{valve} A_v + F_m - F_{sp} \tag{9}$$

Note that the area of the valve term, A_v, in equation (9) is different from the annular flow area of the valve, $A_{v,flow}$, as used in equation (6), this area is explained in the shim stack stiffness model development section.

The momentum force is found by conservation of momentum for the flow through the valve:

$$F_m = \rho \frac{Q_v^{\ 2}}{A_o} \tag{10}$$

Finally, substituting into equation (10) into (9) yields an expression for the valve displacement:

$$ky = \Delta p_{valve} A_v + \rho \frac{Q_v^{\ 2}}{A_o} C_f - F_{sp} \tag{11}$$

The coefficient C_f is included to adjust the magnitude of the momentum term, since the flow field is not completely known. Lang experimentally determined its value to be 0.3. Once the valve stiffness, k, is known, then the deflection can be solved.

The flow rate through the piston orifice is equal to the flow rate through the valving since the valving and the piston orifice are in series. However, there is a different pressure drop between them, namely p_c and p_v in Figure 7:

$$\Delta p_{po} = p_c - p_v \tag{12}$$

Substituting equation (12) into (5) gives the flow rate through the piston orifice, which is equal to the flow rate through the valve:

$$Q_v = A_o C_D \sqrt{\frac{2\Delta p_{po}}{\rho}} \tag{13}$$

BLEED ORIFICE MODEL

To find the pressure drop across the bleed orifice, Bernoulli's equation is applied with a dynamic discharge coefficient:

$$Q_b = A_b C_D \sqrt{\frac{2(p_c - p_r)}{\rho}} \tag{14}$$

In addition, the model has provisions to account for the variability in the area as the needle is adjusted. The area varies between each bleed adjuster setting, because the bleed orifice is a needle valve. The dynamic discharge coefficient was determined experimentally, and the area A_b was calculated for each setting based on measurement taken from the orifice and the tapered needle.

LEAKAGE PAST THE PISTON

Leakage between the piston seal and the cylinder wall, Figure 9, can be modeled as flow between two parallel plates (Lang 1977). This assumes the flow is laminar, which is accurate since the clearance between the cylinder wall and piston is small (less than four thousandths of an inch). The equation for flow between two parallel plates is derived from the Navier-Stokes equations and selecting the correct boundary conditions (Munson, Okiishi, & Young, 1990):

$$Q_{lp} = \left(\frac{\Delta p b^3}{12 \mu l} + \frac{\dot{x} b}{2} \right) \pi D_p \tag{15}$$

where D_p is the diameter of piston and μ is the dynamic viscosity.

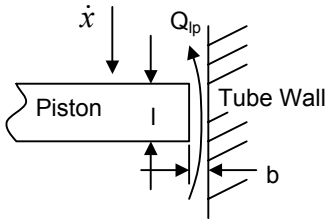

Figure 9: Schematic of Leakage Between the Piston Seal and Tube Wall.

GAS CHAMBER

The gas chamber is designed to account for the volume the rod displaces as it enters the rebound chamber. If the hydraulic fluid is assumed incompressible, then the gas pressure is a function of piston displacement. In addition, a free-body diagram of the gas piston (Figure 10) reveals that the pressure in the compression chamber is related to the gas chamber pressure. It was assumed that the friction between the gas piston and the tube wall was negligible.

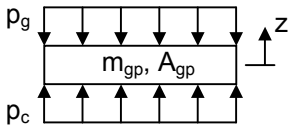

Figure 10: Free-Body Diagram of Gas Piston.

The first step is to determine the pressure in the gas chamber. The ideal gas law is applied and it is assumed that a constant temperature is maintained. This gives an expression for the pressure in the gas chamber:

$$p_g = p_{gi}\frac{A_{gp}L_g}{A_{gp}L_g - A_{rod}x} \tag{16}$$

Now summing forces on the gas piston, Figure 10, and solving for the pressure in the compression chamber:

$$p_c = \frac{m_{gp}\ddot{z}}{A_{gp}} + p_g \tag{17}$$

Assuming the fluid is incompressible it can be shown

$$\ddot{z} = \frac{A_{rod}}{A_{gp}}\ddot{x} \tag{18}$$

Substituting equations (16) and (18) into (17) yields the equation for the pressure in the compression chamber:

$$p_c = \frac{A_{rod}m_{gp}}{A_{gp}^{\ 2}}\ddot{x} + p_{gi}\frac{A_{gp}L_g}{A_{gp}L_g - A_{rod}x} \tag{19}$$

Equation (19) is interesting because it shows that the pressure in the compression chamber is a function of the displacement and acceleration of the piston, but independent of its velocity. Therefore, all of the velocity dependent forces produced by the shock absorber come from the pressure variations in the rebound chamber. This is a key insight into the behavior of this damper design.

SHIM STACK STIFFNESS MODEL

In order to determine the deflection of the shim stack during damper operation it is necessary to accurately predict the stiffness of the shim stack. The model is based on equations for bending of uniform-thickness plates with circular boundaries from Roark and Young (1975). Figure 11 diagrams the approach taken for three shims. If more than three shims are needed, the additional shims would be treated like shim 2 in the figure. The principle of superposition is applied for each shim. The deflection due to the pressure or reaction force at the end of the shim is added to the deflection due to the reaction where one shim contacts another:

$$y_1 = (y_1)_{R_{12}} = (z_2)_{R_{12}} + (z_2)_{R_{23}} \tag{20}$$

$$y_2 = (y_2)_{R_{23}} + (y_2)_{R_{12}} = (z_3)_{R_{23}} + (z_3)_P \tag{21}$$

$$y_3 = (y_3)_P + (y_3)_{R_{23}} \tag{22}$$

The notation $(y_3)_{R_{23}}$ means the deflection y_3 due to the force R_{23}.

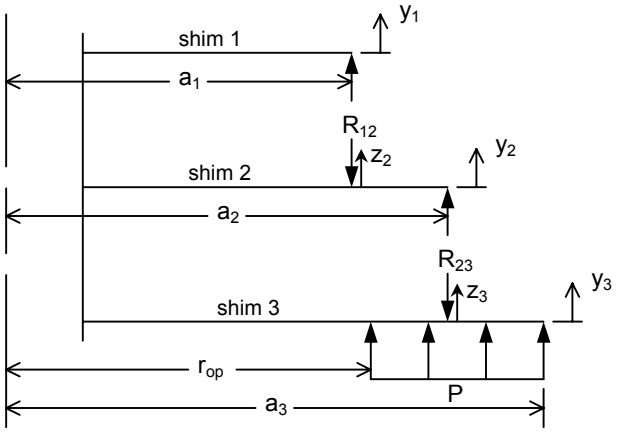

Figure 11: Nomenclature for the Shim Stack Equations.

Now the deflections in equations (20-22) are calculated with equations from Roark. Two cases from Roark were used: one for a line load applied to the circular plate and one for a uniform pressure distribution around the periphery of a circular plate. The line load case is used multiple times; the pressure case is only used for the shim directly against the piston. The result is a system of $5(s-1)-4$ equations, where s is the number of shims. The software implementation of this model can handle a minimum of three shims and a maximum of ten

shims. This is more than adequate for most damper designs.

Several assumptions had to made in developing the shim stack model. First, the radius at which the pressure acts had to be chosen. The radius r_{op} was assumed to be 1.2 times greater than the radius of the top shim, shim 1. The reasons for this assumption were as follows. The top shim is restricted from moving by a large, thick washer on top of it. This washer's stiffness is much greater than the shims, meaning that the deflection y_1 is equal to zero. Thus, the smallest r_{op} could be is the radius of the top shim. The factor of 1.2 was found to work well during the correlation of the model to test data.

In reality the pressure distribution on the bottom shim is probably parabolic in nature, with lowest pressures being at radii a_3 and r_{op}, and the maximum pressure being somewhere in between. However, work has been done using Computational Fluid Dynamics (CFD), which shows that assuming a constant pressure distribution is valid for modeling and will produce accurate results (Herr, et al., 1999).

CFD analysis has also shown that the pressure acting on the shim is confined to a region similar to the size of the piston orifice (Herr et al., 1999). This means that for the piston and valve design modeled, the pressure only acts on roughly half the shim area contained in the circumference between r_{op} and a_3. It also means that only half of the disc circumference would deflect fully. For this reason it was assumed the area of flow through the shim stack only occurs through half of the circumference.

MODEL SOLUTION ALGORITHM

The resulting mathematical model includes six, coupled, nonlinear equations: equations (2,8,11,13-15). The pressure in the compression chamber is known from equation (19) and the total flow rate is given in equation (3). The unknowns are the pressure in the rebound chamber, the three individual flow rates, the deflection of the shim stack, and the pressure in the valve. With the rebound pressure known, equation (1) can be solved for the force generated by the damper given an acceleration, velocity, and displacement. This was done separately for the rebound and compression strokes since the pressure differential definitions change depending on the direction of the velocity.

The solution approach for the system of nonlinear equations is to extend Newton's method to a system of nonlinear equations. Due to the discontinuities in the system, particularly in the region near zero velocity, relaxation techniques are also used in order to solve the system of equations. A description of Newton's method applied to a system of nonlinear equations can be found in Hoffman (1992).

The computer code was programmed in MATLAB and made extensive use of MATLAB's matrix operations. Solving time was approximately twenty seconds depending upon the iteration step size. The computation time is based on a Pentium III processor running at 733 MHz with 128 MB of RAM. It is reasonable to assume that this could be greatly reduced by optimizing the nonlinear system solution algorithm.

MODEL VALIDATION

DAMPER

The damper chosen for the validation work was an Ohlins WCJ 22/6 which is designed for stock car racing, Figure 12. The damper is a mono-tube, gas charged, externally adjustable unit.

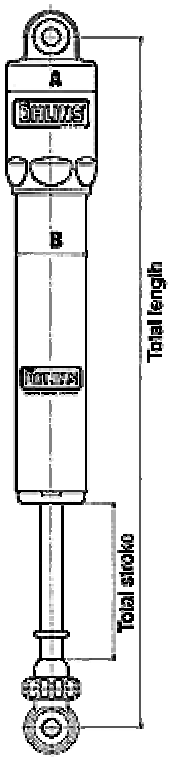

Figure 12: Ohlins WCJ 22/6.

TEST EQUIPMENT

In order to correlate the model it was necessary to test a number of configurations of the damper. A Dynamic Suspensions hydraulic dynamometer was used to carry out the testing, Figure 13. The dynamometer uses a hydraulic linear actuator, a load cell, and a precision displacement transducer. Dynamic Suspensions' DynoSoft 2000 software was used to control the machine and for the data acquisition.

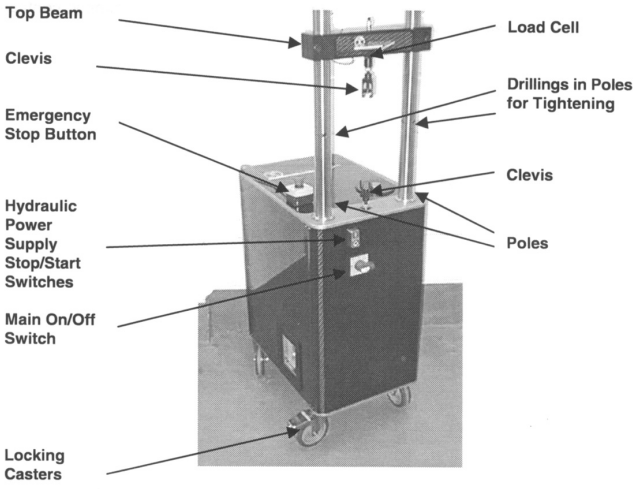

Figure 13: Dynamic Suspensions Hydraulic Damper Dynamometer.

The dynamometer was well suited for this testing with one exception. For the low speed validation the dynamometer is operating near its low speed design limit of 0.4 in/s. At this low speed region, the design of the hydraulics and the control law being used by the dynamometer limits the accurate control of the velocity. Roughness in the velocity data will result in jagged force-velocity (FV) and force-displacement (FD) plots for this low speed region.

TEST METHOD

To verify the computer model it was necessary to perform an extensive series of tests. The test matrix consisted of changing valving, adjuster settings, charge pressure, and stroking amplitude and frequency.

An example test setting is given in Table 1. The damper in Table 1 would be described by denoting its setting as C30 R6 B10. The codes for the compression and rebound valving are listed in Table 2. The C30 compression valving uses six shims, all 0.3 mm thick, ranging in diameter from 19-38 mm (see Table 2, column labeled C30). The adjuster setting refers to the number of clicks open from the fully closed position. The adjuster controls the position of the needle in the bleed orifice. Zero clicks corresponds to fully closed, thirty clicks is fully open; 0, 10 and 30 clicks were tested. The gas charge is the pressure of the nitrogen in the gas chamber when the damper is at full rebound. The amplitude and frequency specify the sine wave stroking profile.

Table 1: Damper Test Setting Example.

Compression Valving	Rebound Valving	Adjuster Setting	Gas Charge (psi)	Total Stroke (in)	Freq (Hz)
C30	R6	B10	145	1.97	1.6

Table 2: Ohlins WCJ Tested Valving Options.

Compression		Rebound	
C30	C70	R6	R70
30-38	30-38	30-36	30-36
30-33	30-36	25-34	25-34
30-30	25-34	20-30	30-33
30-24	20-32	30-26	20-30
30-21	30-30	30-22	30-26
30-19	30-24		30-23
	30-21		30-21
30-38 -->	shim thickness = 0.30 mm shim diameter = 38 mm		

The standard method of testing dampers is to use a sine wave input and control the stroke and frequency. By adjusting the amplitude and frequency, a wide range of desired velocities can be achieved. The damper was stroked about its midpoint for each test. Damper temperature was kept to 20 ± 3 °C for all testing.

MODEL CORRELATION

Several tests were designed to verify the mathematical model. In some cases it was possible to partially isolate a particular equation and verify its accuracy, but it was not possible for others. The main parameters to be verified were the bleed orifice flow path, the valving flow path, and the effect of initial gas charge pressure. Frequency and amplitude of input stroke were also tested; however, the model does not capture the increase in hysteretic effects caused from increasing the frequency.

Bleed Orifice Correlation

The first step in the correlation process was to verify the bleed orifice modeling. The bleed orifice functions at all velocities; therefore its flow properties must be properly captured within the model. To verify the bleed orifice model, the piston orifices were plugged to prevent flow through the piston valving and thus limit the number of parameters influencing the damper's FV and FD characteristics. It will be shown later that the leakage past the piston is insignificant; therefore the primary flow path is the bleed orifice. The model was compared to test data at two bleed orifice settings, 10 and 30 clicks.

The governing equation for flow through the bleed orifice is equation (14). There are three parameters that control this equation: the density of the fluid and the area of the bleed orifice, which were measured, and the dynamic discharge coefficient, C_D. The starting point for determining the discharge coefficient came from Lang's work (1977). He found that the discharge coefficients within the damper he studied were about 0.7. This value was used and then adjusted to get the best correlation between the model and the experimental data. The final value of the dynamic discharge coefficient for the bleed

orifice during compression was 0.61, and 0.69 for rebound. The values are different because the direction flow through the bleed orifice is different for compression and rebound. The values were held constant for all bleed orifice settings and only the area of the bleed orifice was varied.

Figures 14 and 15 are the FV and FD plots for a bleed orifice setting of 30 clicks, and Figures 16 and 17 are for 10 clicks. Overall the agreement between the model and the experimental data is good. However, the model appears to be more nonlinear in nature than the actual damper. One possible cause for this could be compressibility in the fluid, which is not modeled.

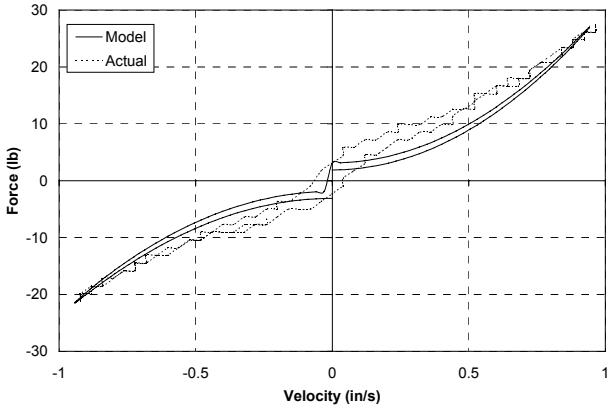

Figure 14: FV Plot for Damper with no Valving and Bleed Set to 30 Clicks.

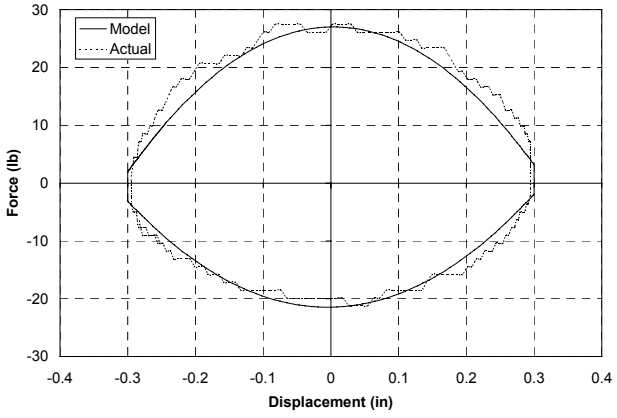

Figure 15: FD Plot for Damper with no Valving and Bleed Set to 30 Clicks.

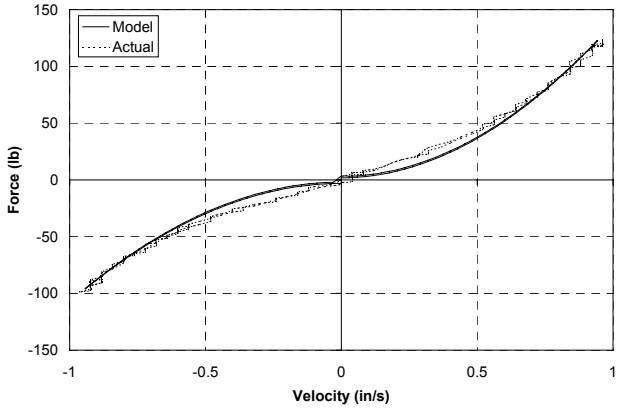

Figure 16: FV Plot for Damper with no Valving and Bleed Set to 10 Clicks.

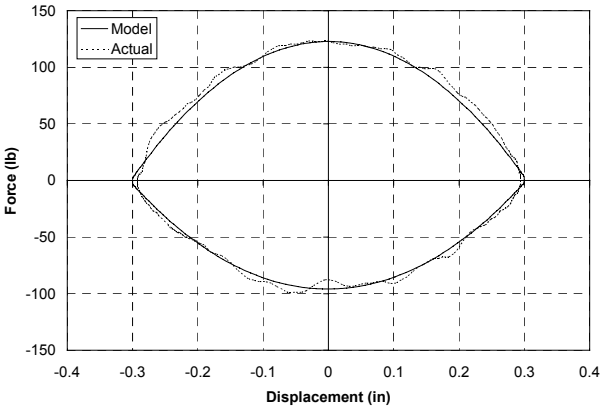

Figure 17: FD Plot for Damper with no Valving and Bleed Set to 10 Clicks.

Valve Correlation

Once confidence was established with the bleed orifice flow parameters, it was necessary to do the same type of correlation for the valve flow. This was accomplished by closing the bleed orifice so that the only flow paths were through the valves and leakage past the piston. It will be shown that leakage past the piston is insignificant; therefore the valves will control the FV and FD characteristics of the damper for this testing.

There are a number of assumptions made that were validated for the valves. The assumptions included the area of the valve on which the pressure acts, the area through which flow occurs, and the dynamic discharge coefficient. The dynamic discharge coefficients were set to 0.7 per Lang's work (1977). The flow areas and the pressure areas, which were assumed in the model development, proved to be accurate enough to achieve

a good correlation. However, the shim stack stiffness model proved to predict high by 8%-15%, which was compensated for by adding an adjustment factor to the shim stiffness calculation. The adjustment factor was set by matching the slopes of the high-speed portions of the FV curves for each shim stack set.

Figure 18 is the FV plot for the shim stack combination of C30 R6 B0. There is very good agreement between the experimental data and the model. The only disagreement is in the zero velocity regions, where hysteresis is evident because the pressures are changing at a high rate. The model does not account for fluid compressibility and therefore doesn't capture the hysteresis.

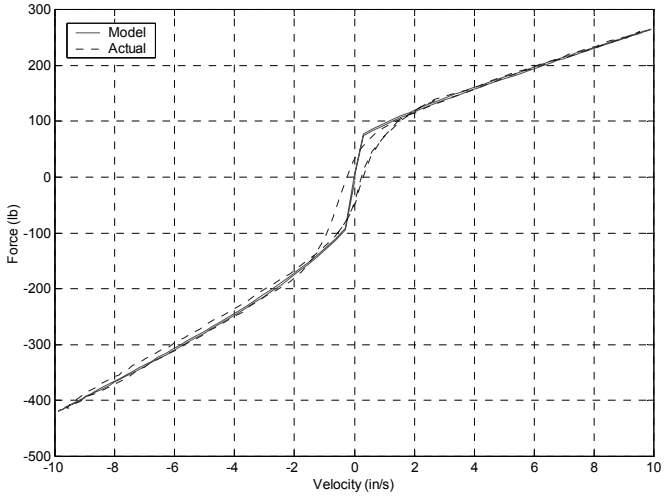

Figure 18: FV Diagram for Valve Correlation, Damper Configuration = C30 R6 B0.

The FD plot for C30 R6 B0 is shown in Figure 19. Again the agreement between model and experimental is very good. The small bump in the experimental data is a control error in the dynamometer and not a damper characteristic.

The same approach was taken to verify the other shim stack combinations, C70 and R70. For the compression shim stacks, C30 and C70, the shim stack stiffness correction factor was set to 0.92. For the rebound shim stacks, R6 and R70, the shim stack stiffness correction factor was set to 0.85. This difference suggests that the assumptions made for the valve pressure and flow areas are off slightly. If the assumptions were correct, the shim stack stiffness correction factor should be the same for all shim stack combinations. The best approach to solve this problem would be to actually measure the shim stack deflection for given pressure differentials. This would be a measurement challenge, however, and was beyond the scope of this study.

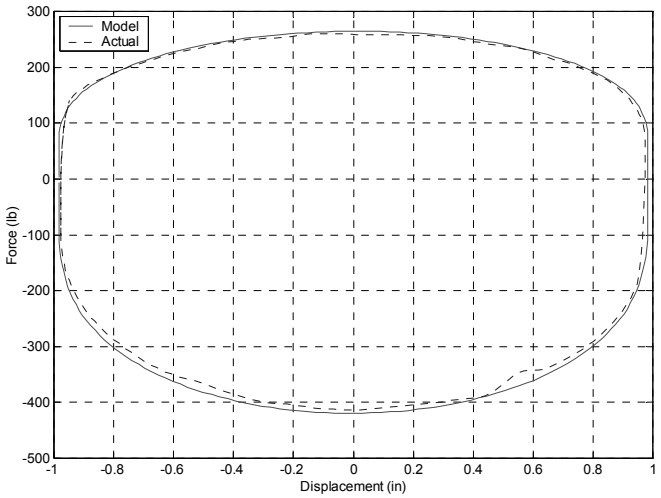

Figure 19: FD Diagram for Valve Correlation, Damper Configuration = C30 R6 B0.

Overall Validation

To achieve an overall model validation it was necessary to test several damper settings with several different run conditions. This was done for all of the shim stacks, C30, C70, R6, R70, at each bleed setting, B0, B10, and B30; all achieved good results. The C30 R6 B30 damper setting will be presented here in detail.

Figure 20 is for a damper setting of C30 R6 B30 and stroking amplitude of 0.984 inches at a frequency of 1.6 Hz. Agreement is very good between the model and experimental data. The only significant difference lies in the low speed region (less than 2 in/s), where the bleed orifice is dominating the damper characteristics. The error in the high-speed region is less than 5%. In compression the low-speed region has an error of up to 50% (although this is only 10 lbs). This difference is shown in Figure 21, which is a low-speed FV plot.

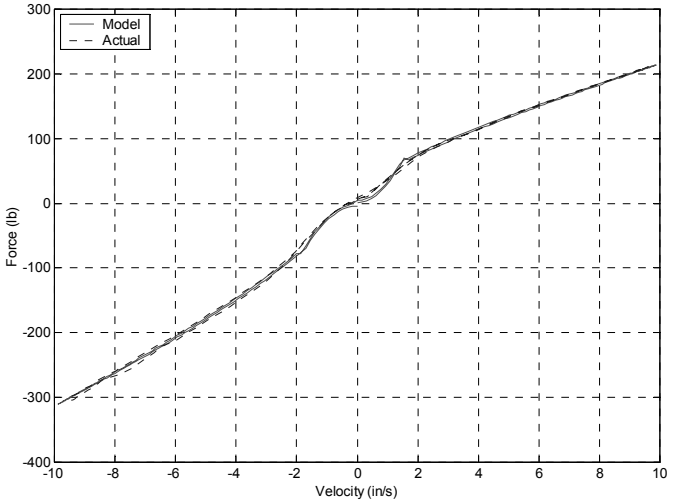

Figure 20: FV Plot for Damper Setting C30 R6 B30: Amplitude = 0.984 in, Frequency = 1.6 Hz.

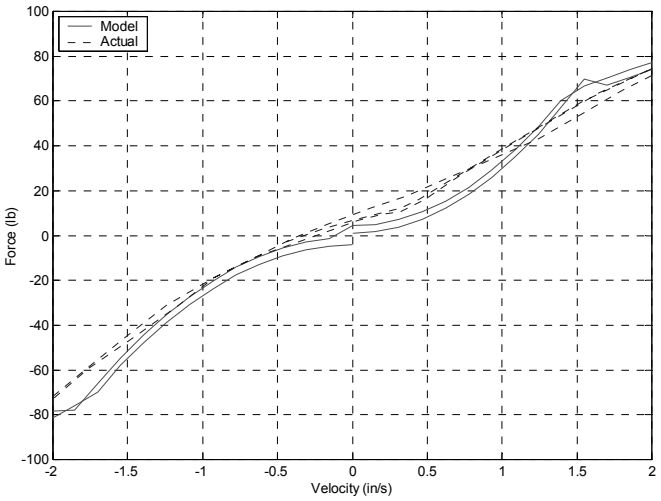

Figure 21: Low-Speed FV Plot for Damper Setting C30 R6 B30: Amplitude = 0.984 in, Frequency = 1.6 Hz.

It is also necessary to study the FD plot to verify that the model is working correctly. It is somewhat easier to verify that the correct force is being generated because the plot clearly separates the accelerating and decelerating portions of the stroke. In Figure 22 the model matches the experimental data very well. The force builds up and falls off at nearly the same rate. The small differences at zero displacement are partly due to the fact that the dynamometer didn't hit the peak velocity called for by the controller. The small bump in the curve in the fourth quadrant on the experimental data is also a result of the dynamometer not producing a smooth, sinusoidal, velocity input.

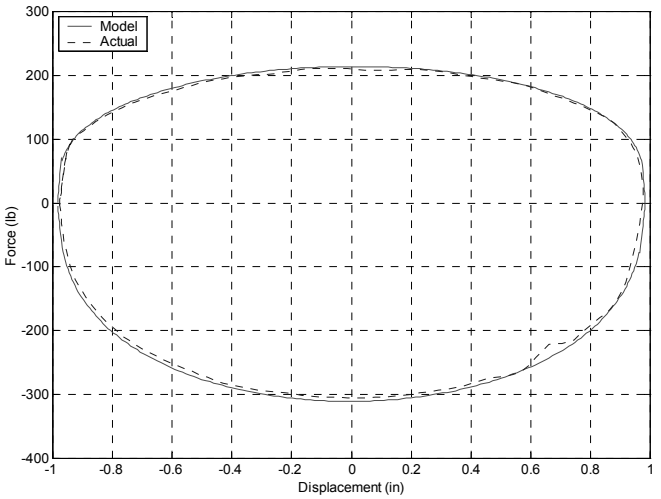

Figure 22: FD Plot for Damper Setting C30 R6 B30: Amplitude = 0.984 in, Frequency = 1.6 Hz.

RESULTS

DAMPER OPERATION

The primary focus of this research was to understand the inner workings of a mono-tube damper. Items of interest include: internal pressures, flow rates through the individual flow paths, shim stack deflection, and the contribution of each flow resistance to the overall damper characteristics. The verified model was exercised to understand the internal phenomena of the damper.

The force generated by the damper is directly proportional to the pressures in the rebound and compression chambers, equation (1). Pressures predicted by the model are shown in Figure 23. The most important insight from these pressures is the fact that the compression chamber pressure is relatively constant. This was predicted by inspection of equation (19); the compression chamber pressure is independent of piston velocity. It is primarily a function of the piston displacement (as seen in Figure 24). The rebound chamber pressure on the other hand, is changing dramatically as a function of velocity. Therefore, it is the pressure variation in the rebound chamber that is controlling the FV relationship of the damper in both rebound and compression.

By studying the valve pressure it is clear that the primary pressure drop occurs across the valve shim stack and not the piston orifice. The pressure within the valve, p_v, is nearly identical to the compression chamber pressure during the compression stroke. This implies that very little pressure drop is occurring across the piston orifice. Likewise, during rebound p_v is nearly identical to the rebound chamber pressure. Again, this indicates the piston orifice is not restricting the flow. This was expected, because the primary tuning mechanism for the damper's high-speed characteristics is the valve shim stack.

Referring again to the rebound pressure in Figure 23, note that the rebound pressure drops considerably during the compression stroke. If the initial gas charge is low enough, the rebound pressure will approach zero and can even go negative (gage pressure). This can lead to cavitation of the fluid and loss of fluid incompressibility. This is one of the main reasons for the development of a gas charged mono-tube damper. The gas charge also acts like a spring, which will be discussed later.

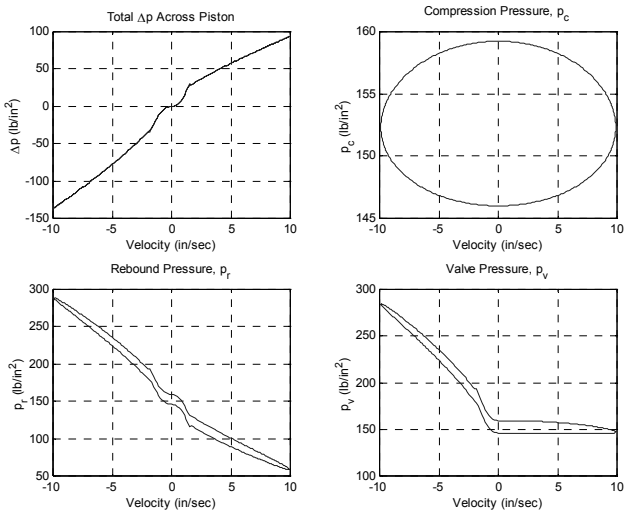

Figure 23: Predicted Pressures of Damper as a Function of Velocity: Damper Setting C30 R6 B30, Amplitude 0.984 in, Frequency 1.6 Hz.

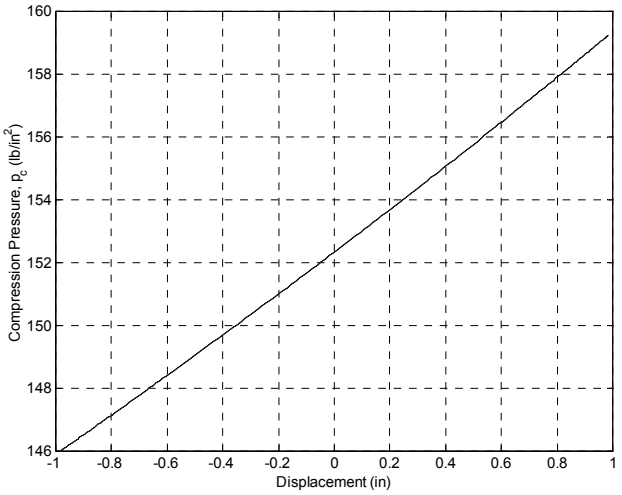

Figure 24: Compression Chamber Pressure Relationship to Piston Displacement: Damper Setting C30 R6 B30, Amplitude 0.984 in, Frequency 1.6 Hz.

The next area of study is the flow rates of the three possible flow paths, Figure 25. First, the total flow rate is directly proportional to piston velocity as was predicted by equation (3). Second, the sum of the individual flow rates is equal to the total flow rate. Looking at any of the three individual flow rates reveals when the valves are opening. The large changes in slope of the curves indicate a change in flow resistance, which happens when the valve opens or closes. In this case the compression valve opens at a velocity of 1.5 in/s, and the rebound valve opens at –1.8 in/s. This corresponds to the deflections of the valves, Figure 26.

The leakage past the piston is insignificant compared to the flow through the bleed orifice and the valves.

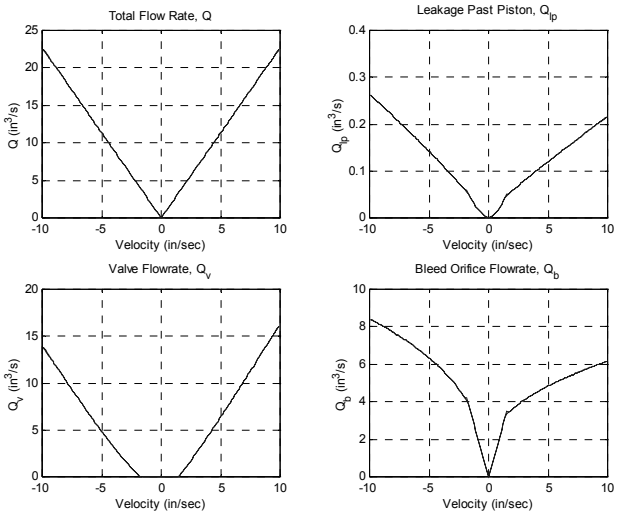

Figure 25: Predicted Flow Rates of Damper as a Function of Velocity: Damper Setting C30 R6 B30, Amplitude 0.984 in, Frequency 1.6 Hz.

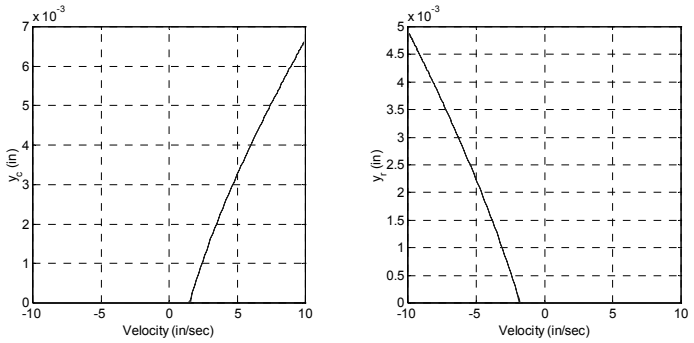

Figure 26: Predicted Valve Deflections as a Function of Velocity.

PARAMETER STUDIES

The model can also be used to perform parameter studies to identify the most important parameters or to tune the damper. The practical parameters of particular interest to a race engineer are: shim stack stiffness, piston orifice area, bleed orifice area, and shim stack preload. These are the primary parameters that would be used to tune the WCJ damper. Therefore, their effect on the FV and FD characteristics needs to be understood.

Other parameters also influence the performance but to a lesser or unknown degree. These parameters will be discussed briefly, and an assessment of their importance will be given. These parameters include: initial gas pressure, mass of the piston, mass of the gas

piston, and friction. Hysteresis will also be discussed briefly.

Shim Stack Stiffness

It was shown that the valve deflection dominates the flow resistance through the valve. Therefore, the shim stack stiffness should have a strong influence on the characteristics of the damper. Figure 27 compares the FV characteristics of the damper with two different valving combinations, C30 R6 B10 and C70 R70 B10. The C30 stack has a calculated stiffness of 5241 lb/in, C70 is equal to 7869 lb/in. The significant difference in stiffness should result is a substantial difference in the FV and FD characteristics during compression. Likewise, the R6 stack has a calculated stiffness of 7638 lb/in, whereas the R70 stack's stiffness is 9181 lb/in. Again, there should be a substantial difference in the FV and FD characteristics.

Figure 27 verifies that indeed valve stiffness is very important in controlling the damper characteristics. However, the valve stiffness only controls the damper characteristics once the valve is open. It also changes when the valve will open because increasing the stiffness increases the preload for the same piston.

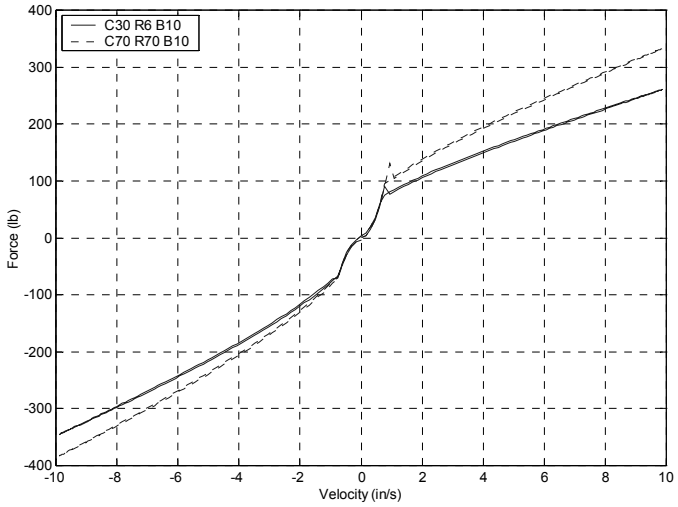

Figure 27: Importance of Shim Stack Stiffness: Predicted FV Characteristic for Two Different Shim Stacks.

Piston Orifice Area

It has been shown, for the piston tested, the piston orifice area had a very small effect on the damper characteristics. This was because the piston orifice area was much greater than the area created when the shim stack deflected. However, different piston designs are available for the WCJ series damper. These different designs change the way the fluid flows through the piston orifice and the pressure distribution on the shim stack, resulting in different damper characteristics. No other piston designs were available to test, but the influence of the piston orifice area was studied with the model.

The specific item of interest was how small the piston orifice area must be to influence the damper performance. Varying the piston orifice area in the model and looking for differences in the damper performance accomplished this. Figure 28 shows the result of this study for the compression piston orifice. The piston orifice area had to be reduced by 50% from 0.0622 in^2 to 0.0311 in^2 to get an appreciable difference in the damper performance.

Another way to look at how the piston orifice area affects the damper is to watch the pressure in the valve. As was discussed in the damper operation section, with the stock piston orifice area there was very little pressure drop across the orifice. The pressure in the compression valve was the same as the pressure in the compression chamber. Figure 29 plots the pressure in the compression and rebound valves for three different compression piston orifice areas. With a 50% reduction in area the valve pressure is not equal to the compression chamber pressure. This indicates that the flow resistance of the piston orifice is significant and would affect damper performance.

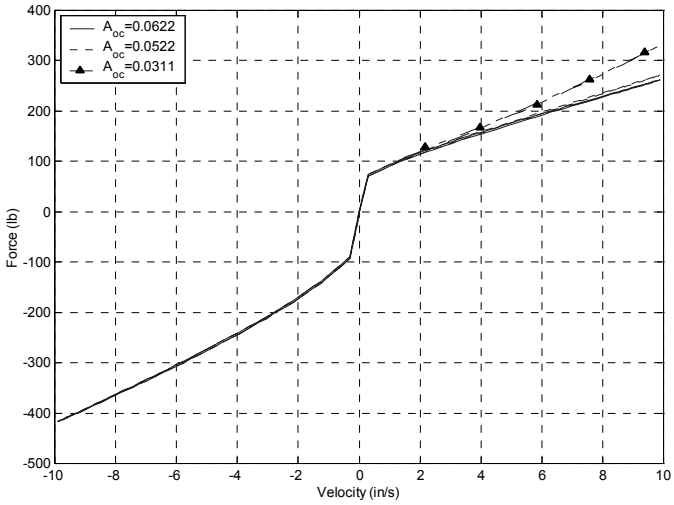

Figure 28: Piston Orifice Area Influence on FV Characteristics.

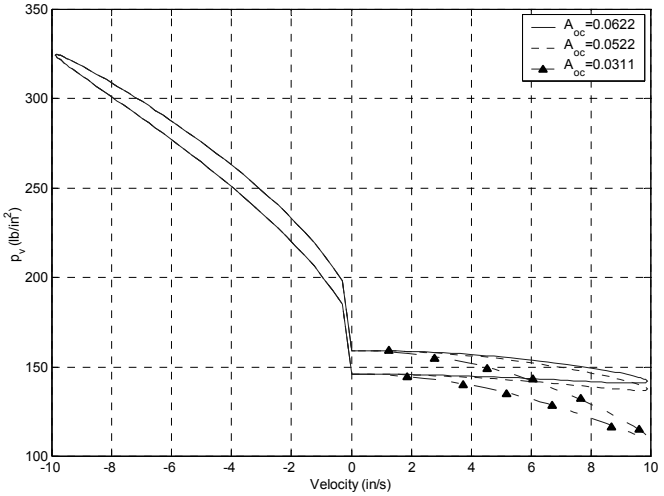

Figure 29: Piston Orifice Area Influence on the Valve Pressure – Compression Only.

Bleed Orifice Area

The only external adjustment for the WCJ series damper is that which controls the bleed orifice area. Figure 30 shows the damper with three different bleed settings: closed, partially open, and fully open. The adjustment dramatically affects the low speed performance of the damper. It also affects the rebound side more than the compression side. This is because the discharge coefficient for flow through the bleed orifice is 0.61 for compression, versus 0.69 for rebound. Therefore, an area change will make a larger difference in rebound because the discharge coefficient is a proportionality factor, equation (14).

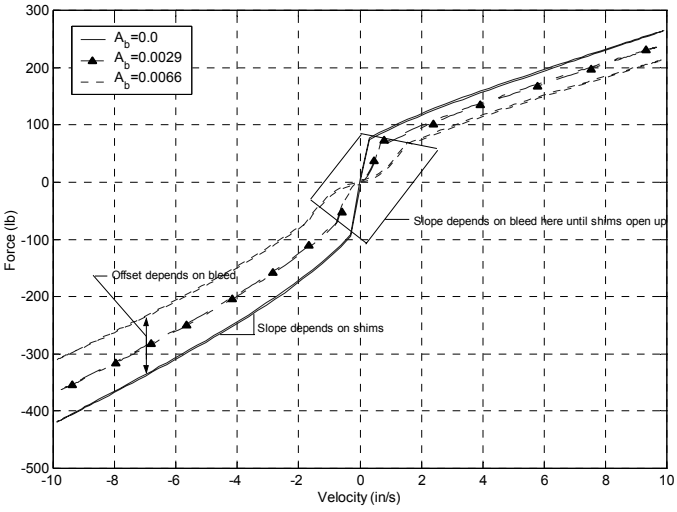

Figure 30: Bleed Orifice Area Influence on Damper Performance: Damper Setting C30 R6 B0, 10, & 30 – B0 = 0.0 in^2, B10 = 0.0029 in^2, B30 = 0.0066 in^2.

The effect of the bleed orifice area can also be seen in a plot of the flow rate through the bleed orifice, Figure 31. For the setting B0, which means the area of the bleed orifice is zero; no flow takes place through the bleed. The difference in flow rate between the three settings is greater for rebound, again because of the smaller discharge coefficient for flow during compression.

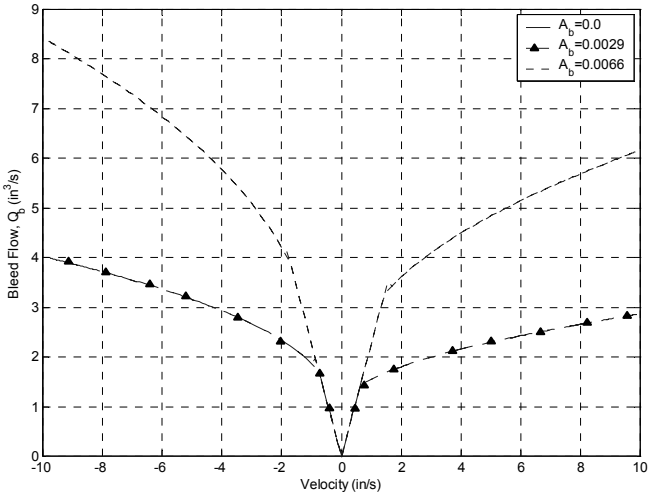

Figure 31: Bleed Orifice Area Influence on Bleed Orifice Flow Rate: Damper Setting C30 R6 B0, 10, & 30 – B0 = 0.0 in^2, B10 = 0.0029 in^2, B30 = 0.0066 in^2. Note: B0 plot is equal to zero at all speeds.

Shim Stack Preload

The shim stack preload is created by the amount of concavity (dishing) on the piston surface where the shim stack contacts the piston. By varying the amount of concavity, usually between one-half and two degrees, the preload on the shim stack can be varied. Increasing the preload, increases the pressure differential necessary to open the valve.

In Figure 32, the preload on the compression shim stack is varied between ten and twenty pounds, in five-pound steps. The five pound change in preload, results in a fourteen-pound change in force over the entire velocity range where the valve is open. The preload setting is a way of offsetting the valve-dominated portion of the FV curve.

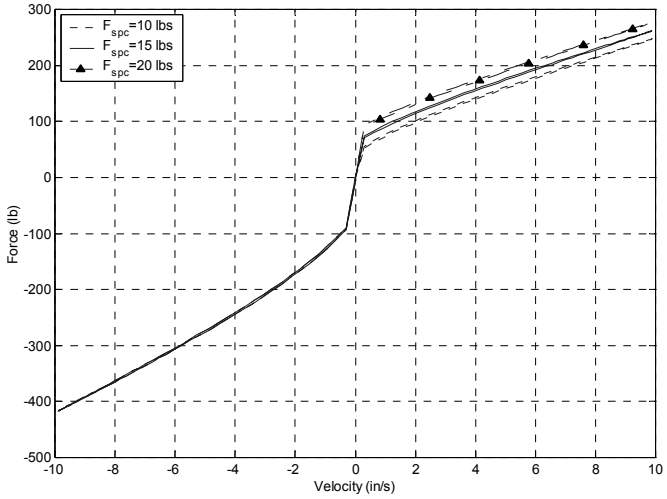

Figure 32: Shim Stack Preload Influence – Compression Valve Only.

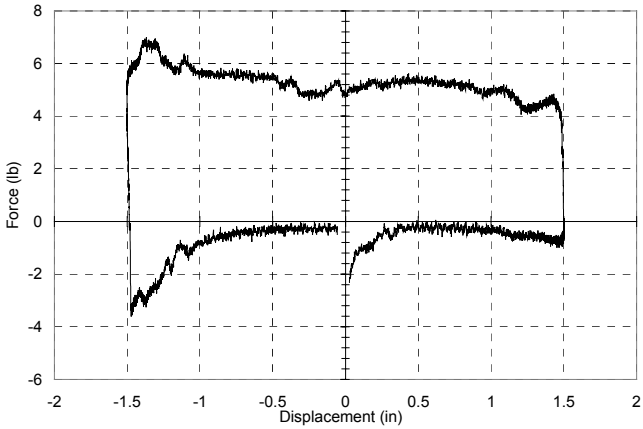

Figure 33: Friction Test for WCJ Damper.

Other Parameters

There are numerous other parameters that are included in the model, but whose influence is minor compared to those parameters already covered. However, their significance is not intuitive and therefore will be discussed briefly.

The initial gas pressure is a very important parameter in mono-tube dampers using a separate floating piston to separate the compression and gas chambers. The gas chamber and gas piston form a gas spring, the stiffness of which is a function of the rod diameter, piston displacement, and gas chamber volume. The main effect of this gas spring is an offset in the FV and FD plots equal to the gas chamber pressure times the rod area. This offset was subtracted out of all the FD & FV figures presented thus far. For the WCJ damper tested the initial gas pressure was set to 140 psi, this equated to an offset force of 43.5 lbs.

The gas pressure will also affect the force output of the damper slightly because the damper will be at different displacements during the accelerating and decelerating portions of the compression and rebound strokes. This difference in displacement causes a small change in the pressure in the gas chamber, which in turn changes the force resulting from the gas pressure time the rod area.

Friction was measured for the damper and found to be very low relative to the force generated by the damper. Only at extremely low velocities would it be significant. Figure 33 is a FD plot for the friction test performed on the damper. For this test all of the shims were removed and the bleed was fully open so that there was very little restriction to flow. Damper speed was kept below 0.2 in/s for the test. The results are interesting, because it appears the damper has more friction during compression than for rebound. The cause of this is not known, but likely is due to the rod seal design.

Finally, hysteresis should be briefly discussed. Although the model makes no attempt to capture this phenomenon, it is worth mentioning so that the effect of frequency on dampers is understood. Figure 34 is a FV plot of test data for the same damper setting (C70 R70 B0), with the same velocity input, but at different frequencies. The low frequency plot is 1.6 Hz; the high frequency plot is at 8.0 Hz. The velocity is maintained by changing the stroke. Notice the significant difference in the width of the hysteresis loop. The rapidly changing pressure in the rebound chamber and the compressibility of the fluid causes this difference. The model assumes the fluid is incompressible and therefore, does not capture this hysteretic effect. In reality the damper fluid is compressible and will contain a small amount of entrained air, which increases the compressibility.

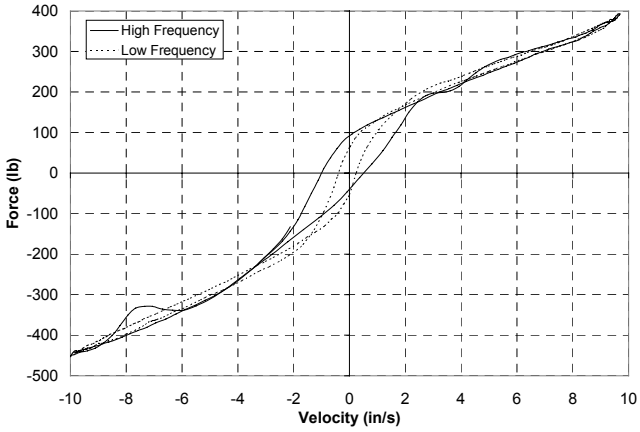

Figure 34: Frequency Effect on Hysteresis Loop Width.

CONCLUSIONS

The model accurately predicts the FV and FD characteristics of the WCJ damper. Testing indicated that the model could cover a wide range of damper settings, which included different valves and bleed orifice settings.

One of the most significant insights from this modeling exercise is that the pressure in the compression chamber stays nearly constant throughout the stroke. The pressure in the rebound chamber varies a great deal, however. This means that the pressure in the rebound chamber is responsible for generating the pressure differentials across the piston, which in turn generates the damper's performance characteristics.

Another significant contribution of this work is the shim stack deflection modeling. Using circular models of thin plates stacked upon one another is a reasonable and accurate way to model the effects of shims and to model the piston valves.

The most significant damper parameters were identified and studied in detail. Bleed orifice properties dominate the low speed regime, while the high-speed regime is dominated by the shim stack stiffness. However, if the piston orifices are reduced in size they will influence the high-speed characteristics of the damper.

There are several areas for further work to improve the model. These include: fluid compressibility effects, temperature compensation, and improvement in the low speed bleed orifice flow model. Tuning the numerical algorithm would also reduce computation time, which would be necessary to include this model in a vehicle simulation.

ACKNOWLEDGMENTS

The authors would like to thank the following companies for their support of this research: Ford Motor Company, Honda R&D Americas Inc., and Ohlins USA Inc.

REFERENCES

1. Audenino, A.L. and G Belingardi, 1995, "Modelling the Dynamic Behaviour of a Motorcycle Damper," Proceedings of the Institution of Mechanical Engineers. Part D, Journal of Automobile Engineering, v 209 n 4, pp. 249-262.
2. Bergen, C., 2000, Ohlins Representative, Personal Conversation, Feb. 15, 2000.
3. Dixon, J. C., 1999, The Shock Absorber Handbook, SAE, Warrendale, PA.
4. Duym, S.W., R. Stiens, G.V. Baron, and K.G. Reybrouck, 1997, "Physical Modeling of the Hysteretic Behaviour of Automotive Shock Absorbers," SAE Paper 970101.
5. Gillespie, Thomas D., 1992, Fundamentals of Vehicle Dynamics, SAE, Warrendale, PA.
6. Herr, F., Mallin T., and Roth S., 1999, "A Shock Absorber Model Using CFD Analysis and Easy5," SAE Paper 1999-01-1322.
7. Hoffman, Joe D., 1992, Numerical Methods for Engineers and Scientists, McGraw-Hill, New York.
8. Hoffmann, H. J., 1958, "Wirkameseit von Stossdampfern am Fahrzeug," (Effectiveness of Shock Absorbers on Vehicles), Automobiltechnische Zeitschrift, J60, H10.
9. Lang, H. H., 1977, "A Study of the Characteristics of Automotive Hydraulic Dampers at High Stroking Frequencies," Ph.D. Dissertation, The University of Michigan.
10. Milliken, William F. and Douglas L. Milliken, 1995, Race Car Vehicle Dynamics, SAE, Warrendale, PA.
11. Munson, B.R., Okiishi, T.H., and Young, D.F., 1990, Fundamentals of Fluid Mechanics, 2nd ed, John Wiley & Sons, New York.
12. Reybrouck, K, 1994, "A Non Linear Parametric Model of an Automotive Shock Absorber," Vehicle Suspension System Advancements, SAE Paper 940869.
13. Roark, R.J. and Young, W. C., 1975, Formulas for Stress and Strain, 5th ed., McGraw-Hill, New York, pp. 324-343.
14. Segal, L. and Lang, H. H., 1981, "The Mechanics of Automotive Hydraulic Dampers at High Stroking Frequencies," Vehicle System Dynamics, No. 10, pp. 82-85.
15. Talbott, M.S. 2002, "An Experimentally Validated Physical Model of a High-Performance Automotive Damper," MS Thesis, Purdue University.
16. Ohlins NASCAR Winston Cup Shocks: Racing Workshop Manual, 4th ed., 1997.

CONTACT

Michael Talbott, Honda R&D Americas, Inc., 21001 State Route 739, Raymond, OH 43067. Email: mtalbott@oh.hra.com, talbotms@hotmail.com

John Starkey, Purdue University, 1288 Mechanical Engineering Bldg., Purdue University, West Lafayette, IN 47907. Email: starkey@ecn.purdue.edu

DEFINITIONS, ACRONYMS, ABBREVIATIONS

A: area

A_b: area of the bleed valve orifice

A_c: area of the compression side of piston

A_{gp}: area of the gas piston

A_o: area of the piston orifice

A_r: area of the rebound side of piston

A_{rod}: area of the rod

A_v: area of the valve on which the pressure acts

$A_{v,flow}$: area through which valve flow occurs

b: clearance between piston and cylinder wall

C_D: dynamic discharge coefficient

C_f: momentum adjustment coefficient

D_p: diameter of piston

D_v: diameter of valve

E: modulus of elasticity

F: damper force

F_f: friction force from seals

F_m: momentum force on the valve caused by the fluid changing direction

F_{sp}: preload force on shim stack

k: shim stack stiffness

l : length of leakage gap

L_g: length of gas chamber

m_{gp}: mass of the gas piston

m_p: mass of piston/rod assembly

p: pressure

p_c: pressure in compression chamber

p_r: pressure in rebound chamber

p_v: pressure within the valving

Q: total volumetric flow rate

Q': equivalent flow rate due to rod insertion

Q_b: flow rate through bleed orifice

Q_{lp}: leakage flow between piston and cylinder wall

Q_v: flow through valve

r: radius of cylinder cross section

t_w: wall thickness of cylinder

v_y : fluid velocity through the valve in the y-direction

x : piston displacement

$\dot{x}$: piston velocity

$\ddot{x}$: piston acceleration

y : valve opening distance

z : gas piston displacement

$\ddot{z}$: gas piston acceleration

β: fluid compressibility

β': effective compressibility including cylinder wall compliance

Δp: pressure differential

Δp_{po}: pressure differential across the piston orifice

Δp_{valve}: pressure differential across valve shim stack

μ: dynamic viscosity

ρ: density